Continuum Mech. Thermodyn.
https://doi.org/10.1007/s00161-023-01268-y

S.I. : EXPERIMENTAL INVESTIGATIONS AND MODELLING IN POLYMER MECHANICS

Sameer Kulkarni · Marie-Christine Reuvers · Tim Brepols · Stefanie Reese · Michael Johlitz · Alexander Lion

Characterization of crystallization kinetics in Polyamide 6 with a focus on modeling the thermoforming process: experiments, modeling, simulations

Received: 27 May 2023 / Accepted: 19 October 2023

Abstract Thermoforming of continuous fiber-reinforced plastics made of semi-crystalline thermoplastics has gained significant interest due to its potential for producing lightweight and high-strength components for various applications. Before thermoforming, a laminate is heated to a temperature beyond the melting point of the thermoplastic. During the subsequent forming process, the laminate is continuously cooled, which triggers non-isothermal crystallization in the semi-crystalline matrix material. In this context, the study of crystallization kinetics is crucial in identifying phase transition, analyzing exothermic latent heat during crystallization and determining inhomogeneous crystallinity distribution caused by uneven cooling in the laminate's thickness direction. This contribution primarily deals with experimental investigations, modeling and finite element simulations for characterizing the crystallization kinetics in the matrix material, Polyamide 6 and investigating the aforementioned factors. To model the crystallization kinetics, an extended form of the Avrami model, known as the modified Nakamura–Ziabicki model, is adopted. The parameters for the modified Nakamura–Ziabicki model, which depend on the local cooling rates, are identified based on fitting the model to flash DSC (differential scanning calorimetry with high cooling rates) and standard DSC non-isothermal cooling experiments. Finally, the model is implemented into the commercial FE software COMSOL Multiphysics® and the crystallinity evolution in the laminate is simulated for the process-relevant die and laminate temperatures and laminate thicknesses.

Keywords Thermoforming · Crystallization kinetics · F-DSC · PA6 · CoFRTP · FE analysis

Communicated by Andreas Öchsner.

S. Kulkarni (✉) · M. Johlitz · A. Lion
Institute of Mechanics, University of the Federal Armed Forces Munich, Werner-Heisenberg-Weg 39, 85577 Neubiberg, Germany
E-mail: sameer.kulkarni@unibw.de

M. Johlitz
E-mail: michael.johlitz@unibw.de

A. Lion
E-mail: alexander.lion@unibw.de

M.-C. Reuvers · T. Brepols · S. Reese
Institute of Applied Mechanics, RWTH Aachen University, Mies-van-der-Rohe-Str. 1, 52074 Aachen, Germany
E-mail: reuvers@ifam.rwth-aachen.de

T. Brepols
E-mail: tim.Brepols@rwth-aachen.de

S. Reese
E-mail: stefanie.reese@ifam.rwth-aachen.de

Published online: 22 November 2023

1 Introduction

Continuously fiber-reinforced polymers (CoFRP) have emerged as a promising material in recent years, offering excellent mechanical properties with a high potential for lightweight design. This property has made CoFRP a popular choice in automotive and aviation industries, where weight reduction is a critical factor in improving fuel efficiency and reducing emissions [1,2]. In addition to their superior mechanical properties, CoFRP offer a number of other advantages. They are also highly customizable, with a range of fiber and matrix materials available to suit different applications and they can be formed into complex stuctures.

Continuous fiber-reinforced thermoplastic polymers (CoFRTP) are a class of engineering materials that are comparatively new in the field, especially when compared with their thermosetting counterparts. Thermoplastics are known to have a significantly higher melt viscosity in the range of 10^2–10^4 Pa s, as compared to thermoset resins. This higher viscosity poses a number of challenges during the forming process, such as inadequate impregnation of reinforcing fibers with the matrix, insufficient adhesion of plies and less efficient void removal during consolidation. Additionally, it affects the flow of resin during the forming process [3]. Thermoplastic composites exhibit numerous advantages when compared to thermoset composites, including superior ductility, impact resistance and the ability to be recycled. Besides these advantages, these materials possess remarkable mechanical and thermal properties [4,5]. The increasing emphasis on reducing carbon footprint and achieving lightweight requirements has propelled the rapid development of CoFRTP in the automotive industry and aerostructures [3]. The aforementioned differences render CoFRTP laminates a highly desirable material for the large-scale manufacturing of superior-grade structures [5].

The process of thermoforming CoFRTP is gaining importance due to its speed and material efficiency [6]. The thermoformed CoFRTP usually comprise semi-crystalline thermoplastics due to their superior mechanical properties to amorphous thermoplastics [3]. Semi-crystalline polymers belong to a specific category of thermoplastics, which partially crystallize as they cool down from the molten state. In the thermoforming process, a pre-consolidated laminate made of thermoplastic unidirectional (UD) tapes known as an organosheet is heated using infrared technology until it melts. Then it is transported into a forming press where a die and a punch, which are at lower temperatures than the pre-consolidated laminate, shape it into the desired form. Finally, a compaction stage consolidates the final composite part [7]. To make sure that thermoformed parts with complex shapes will have the desired mechanical properties and be technically feasible, it is important to use numerical simulations to predict how the forming process will work [7]. Proper selection of the processing parameters (e.g., tool and laminate temperatures or forming speed) obtained from such simulations, can help to ensure consistent and optimal properties of the final part.

Thermoforming simulation of CoFRTP has recently been approached by assuming the process to be isothermal due to the limited forming time of 1 to 10 s [8]. However, some studies such as [9,10], have considered the thermal behavior and temperature-dependent mechanical behavior in terms of a thermomechanical coupling. Nevertheless, these studies have been limited to temperatures above the onset of crystallization, which marks the beginning of the transition from a molten state to a solid state and induces a significant increase in the material stiffness. The morphology of the underlying microstructure, including the degree of crystallinity, crystal configuration and lamellae thickness, has a significant impact on the mechanical properties of semi-crystalline polymers [11,12]. Recent experiments conducted by the authors of this article also show that the mechanical and thermal response of the semi-crystalline polymer PA6 varies significantly as a function of the degree of crystallinity. The thermoforming simulation approach by Dörr [6] accounted for crystallization kinetics in terms of crystallization onset and latent heat of crystallization. However, the variation of physical properties based on the degree of crystallinity, which can differ greatly by tens of percentages due to the varying local cooling rate, were not considered. The mechanical properties, including shrinkage, impact behavior and stiffness, as well as the optical properties of a material are markedly impacted by the degree of crystallinity [13].

In [12], Felder et al. derived a thermodynamically consistent viscoelastic, elastoplastic framework for semi-crystalline polymers to simulate the cooling of the molten material and subsequent loading in the solid state. This framework incorporated the crystallinity dependency on the mechanical properties of the solidified material. However, the range of crystallinities that the authors evaluated was very narrow, only 5% (from 23 to 28%). This range is unfortunately not representative of the broad spectrum of crystallinities that can result from cooling rates typically observed during thermoforming, ranging from 1 to 150 °C s^{-1} [8].

Within the framework of this project, initial predictions were made for the process-relevant range of local cooling rates occurring in the laminate, as well as the resulting degree of crystallinities. These predictions were based on simplified finite element simulations [14]. The project aims to broaden the scope of Felder's

material framework [12] to encompass a wide range of crystallinities and to integrate anisotropy into the model by accounting for the fiber contribution. The unidirectional composite layers shall be modeled transverse isotropically based on the approach of structural tensors. Using this thermomechanically coupled material framework, it will be possible to simulate the entire end-to-end thermoforming process. Regarding the current advancements in the material model, the reader is referred to [15].

This particular contribution focuses solely on thermal modeling, specifically on crystallization within the matrix during the cooling of a composite laminate. The mechanical effects, such as pressure, are neglected within the scope of this study. In the case of semicrystalline polymers, the temperature at which the material crystallizes during cooling is typically lower than the melting temperature during subsequent heating. This difference for PA6 typically falls within the range of 20°–30°, as observed in the flash DSC results depicted in Figs. 3 and 4. This implies that for the newly formed crystallites to remelt, the temperature must rise by at least 20 °C due to the exothermic heat released during crystallization. In a study involving the cooling of a PA6 laminate, as described in [16], it was observed that the crystallization did induce a slight reduction in the cooling rate but did not result in a temperature increase. Hence, a simple crystallization model that allows only the progress of crystallization during cooling can be used, provided that the simulated temperature does not exceed the melting point during and after crystallization. A modified form of the Avrami model, known as the modified Nakamura–Ziabicki model, is adopted to model the crystallization kinetics under this assumption. The model is calibrated using non-isothermal F-DSC (flash DSC) and S-DSC (standard DSC) experiments. Finally, the model is implemented into the commercial FE software COMSOL Multiphysics® and the crystallinity evolution in the laminate is simulated for the process-relevant die and laminate temperatures. In summary, the incorporation of the crystallization kinetics model in this study serves to achieve the following objectives:

- to identify the phase transition from the molten to the solid state,
- to consider the exothermic latent heat release during crystallization in the thermal analysis,
- and to simulate the nonhomogeneous crystallinity distribution in the laminate resulting from uneven cooling in the thickness direction.

2 Experimental investigations

The goal of this investigation is to characterize the crystallization behaviour primarily during cooling from the melt for a wide range of cooling rates, which are observed during thermoforming. To gain information about crystallization, experiments using F-DSC and S-DSC were performed. The composite material under investigation consists of a unidirectional glass fiber reinforcement and a polyamide 6 (PA6) matrix, which is also commonly known as nylon 6. The experiments were conducted on PA6 instead of the composite due to the utilization of F-DSC, where the sample's mass is on a nanogram scale, making it unfeasible to control the precise fiber proportion in the samples. S-DSC was used for low to moderate cooling rates from 0.033 to 1 °C s^{-1}, whereas F-DSC was used for moderate to high cooling rates from 0.25 to 3000 °C s^{-1}. The PA6 under investigation is an industrial grade from the company LANXESS. The density of the material at room temperature was 1.14 g cm^{-3}, measured with a gas pycnometer with an accuracy of less than 0.1%. Before testing, the specimens were stored in a dry chamber (MP Dry Cabinet IV ST) at 40 °C until their moisture content was less than 0.1%.

The S-DSC measurements were conducted using an in-house machine Q2000 from TA instruments for the following low to moderate cooling rates 0.033, 0.083, 0.167, 0.250, 0.333, 0.5, 0.667, 0.833 and 1 °C s^{-1}. Open aluminium crucibles were used for the experiments and the specimen weighed approximately 5 mg. The sample was in each cycle first held isothermal at 30 °C, then heated with a heating rate of 10 °C s^{-1}, up to 280 °C and held there for 2 min. The sample was then cooled down to 30 °C using different cooling rates as specified earlier. In Fig. 1, the cooling S-DSC result signals are shown.

When the material changes from a liquid to a solid state, it releases latent heat, which creates a heat flow signal that looks like a Gaussian bell-shaped curve. As the cooling rate increases, the crystallization start temperature and peak temperature decrease. The enthalpy of crystallization, which is the amount of energy released during this process and represented by the area under the bell-curve, when plotted heat flow against time, also decreases while the curve becomes wider. At lower cooling rates, the curve looks symmetrical, but it becomes asymmetrical at higher cooling rates. It is important to note that this effect is not a result of the material behavior but rather due to the sample mass being too large for uniform crystallization throughout the sample. This phenomenon is well-known among DSC users and can be resolved by reducing the sample mass.

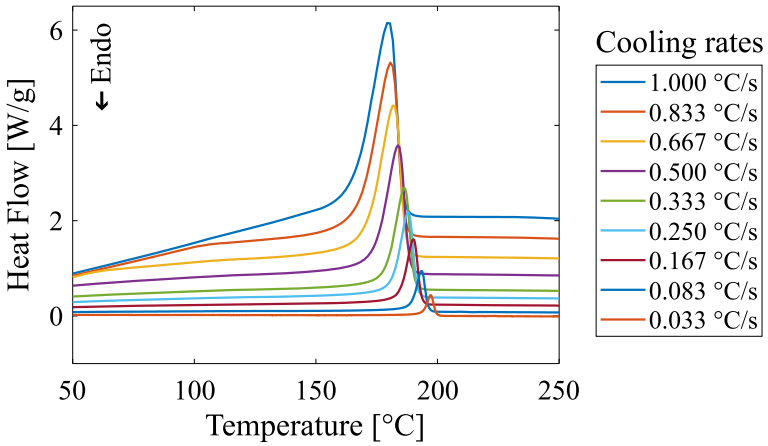

Fig. 1 Results of S-DSC cooling runs for low to moderate cooling rates

However, in this case, the sample mass used is already considered small in standard DSC equipment, leaving no apparent solution to the problem [17].

The F-DSC technique allows heating and cooling at very fast rates, which are not possible in the S-DSC method. This is due to the extended time required to heat or cool samples with a large mass used in the S-DSC. The typical sample mass in a F-DSC 1 device from Mettler-Toledo is between 5 and 100 ng. As a result, heating and cooling rates of several 1000 °C s^{-1} can be achieved [18]. Typical heating rates, according to the product manual of F-DSC 1, are between 1 and 40,000 °C s^{-1} and typical cooling rates are from 1 to 4000 °C s^{-1} [19]. For more information about F-DSC, the reader is referred to [19]. Fast differential scanning calorimetry (F-DSC) experiments were commissioned by Professor René Androsch at the University of Halle, Germany, using a Flash DSC 1 device to investigate cooling rates ranging from 0.25 to 3000 °C s^{-1}.

The degree of crystallization in the material after the cooling process is directly proportional to either the specific crystallization enthalpy evaluated from the cooling curve or the specific melting enthalpy obtained from the subsequent heating curve. The evaluation of crystallization peaks is usually more prone to experimental errors; therefore, heating curves are generally preferred for a more reliable analysis [13]. However, the latter method has a significant limitation. Any unstable phases present in the initial material after cooling can reorganize into more stable phases during the subsequent heating scan in DSC. This process is also known as cold-crystallization. As a result, the final melting endotherm is not a reliable indicator of the actual structure of the material since it represents both the melting of the initial crystals formed during cooling and the reorganized phases [20]. The study in [21] compared the differences in the final morphology of cold-crystallized and melt-crystallized crystallites using WAXS (wide-angle X-ray scattering) experiments and AFM (atomic force microscopy). The study also provided insights into the various nucleation mechanisms involved. In [22], Khanna and Kuhn discussed the challenges that arise during DSC heating and provided solutions for measuring the crystallinity of PA6 without introducing measurement errors in cases where cold crystallization occurs. A way to prevent measurement error during the DSC heating cycle is to employ a high heating rate, which suppresses cold crystallization; the process is also known as complete vitrification [23]. In this scenario, only the initial crystals melt without any reorganization of the crystal structure and only one melting peak is observed. This single peak, in this case, more accurately represents the melting behavior of the crystals that were formed during the production process [18,24].

Mathot et al. [25] conducted a study where PA6 material was cooled at varying rates from the molten state using F-DSC experiments. It was subsequently heated back to its molten state at two distinct rates for each previous cooling rate [25]. These experiments showed that the higher the cooling rate from the melt and the suppression of hot crystallization, the higher the cold crystallization observed in the subsequent heating cycle. Hence, to identify the critical heating rate required to prevent cold crystallization, a preliminary test was conducted in analogy to the above test. In this test, the specimen was first melted by heating it to 250 °C. Then it was repeatedly cycled between 250 and −60 °C. The cooling was done with a constant and very high rate of 3000 °C s^{-1}, for a reason stated earlier. However, the heating rate was changed in each cycle, varying from 1 to 1000 °C s^{-1}. The sample was held isothermal at the highest and the lowest temperatures for 0.5 s. Figure 2 presents the results of this test. In this plot, the DSC signals are rate normalized, meaning each heat flow curve is divided by the corresponding heating rates, so the area under each bell-shaped curve represents the actual cold crystallization or the melting enthalpy.

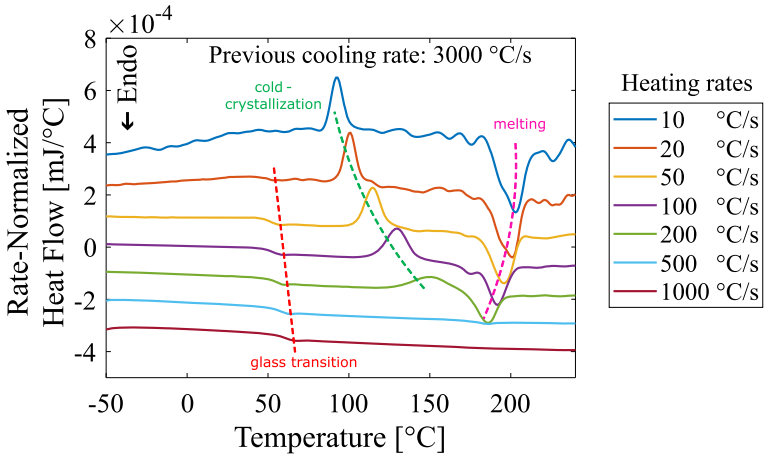

Fig. 2 Pre-Test to determine the critical heating rate after cooling at 3000 °C/s with F-DSC

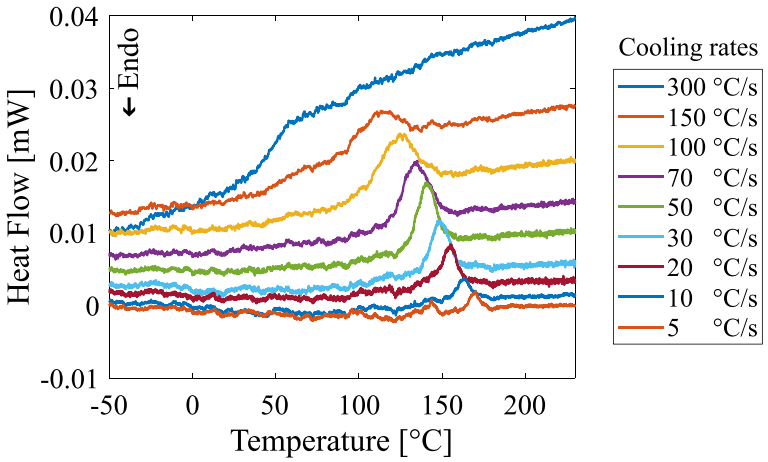

Fig. 3 Results of F-DSC cooling runs for moderate to high cooling rates

During the heating cycle of a DSC measurement, the heat flow curve shows three distinct phenomena: glass transition, cold-crystallization and melting. The glass transition is detected as a sudden step in the curve around 50–70 °C. This is followed by an exothermic peak indicating cold-crystallization and finally, an endothermic peak indicating melting of the material. The cooling rate of 3000 °C s^{-1} is too fast for PA6 to crystallize and it remains in an amorphous state. Therefore, when the material is heated again, the peak indicating cold crystallization appears almost the same size as the melting peak. At increasing heating rates, the cold crystallization peak in the DSC curve moves to higher temperatures. On the other hand, the endothermic melting peak moves towards lower temperatures. This happens because the crystallites have less time to grow during heating, making them smaller in size, which causes them to melt earlier [18]. It is observed that at a heating rate of 500 °C s^{-1}, there is a significant suppression of crystallization. At a heating rate of 1000 °C s^{-1}, both peaks become almost nonexistent. Therefore, the critical heating rate should fall within the range of 500 °C s^{-1} to 1000 °C s^{-1}. For future experiments that investigate the crystallization kinetics during cooling, the upper limit of 1000 °C s^{-1} is used. This choice of a higher heating rate ensures that the cold-crystallization, which impacts the measurement of crystallinity, is prevented. In [26], the critical heating rate for fully amorphous samples is reported to be 500°C s^{-1}.

After determining the critical heating rate, the actual F-DSC cooling experiments were conducted to study the kinetics of cooling crystallization. The sample was cycled between 250 and −60 °C, with the heating rate held constant at 1000 °C s^{-1} while the cooling rate varied in each cycle. The cooling rates tested were 0.25, 0.5, 1, 3, 5, 7, 10, 15, 20, 30, 50, 70, 100, 150, 300, 1000 and 3000 °C s^{-1}. The sample was held isothermal at the highest and lowest temperatures for 0.5 s. The results of the cooling and the subsequent heating runs are presented in Figs. 3 and 4, respectively.

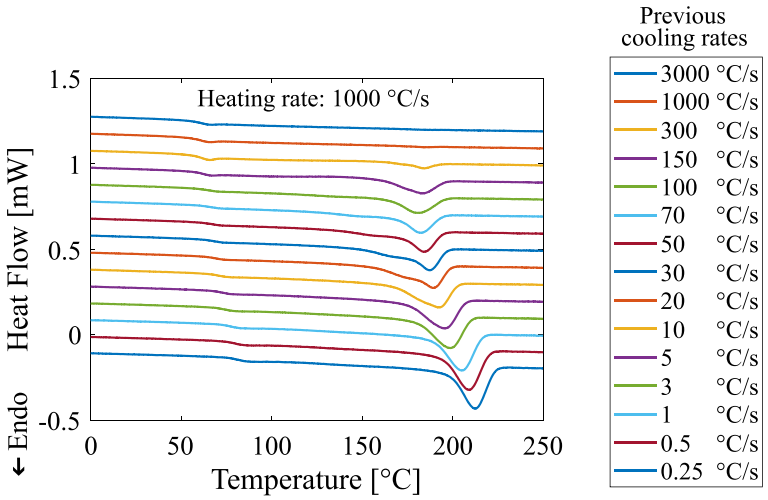

Fig. 4 Results of F-DSC heating runs after cooling with temperature rates specified

At low cooling rates ranging from 0.25 to 3 °C s^{-1} (equivalent to 15 and 180 K min^{-1}), the signal-to-noise ratio, as seen in Fig. 3, is relatively low owing to the low sample mass. Unfortunately, due to the small size of the specimens, the mass of the samples cannot be determined using conventional gravimetric tools. On the contrary, the signal-to-noise ratio in the heating curve, as illustrated in Fig. 4, is substantially higher. Therefore, measuring the crystallization enthalpy through the heating curve is clearly a more favorable approach.

As seen in Fig. 4, the enthalpy of crystallization, which is quantified by the area under the bell-shaped melting curve, decreases continuously with increasing cooling rate and ultimately gets zero if the cooling rate reaches 1000 °C s^{-1}. Several authors reported the critical cooling rate required to restrict crystallization or achieve complete vitrification is slightly lower (around 100–500 °C s^{-1}) [21,24–27]. The observed discrepancy is believed to be attributed to several factors, including differences in structural composition, the presence of additives and nucleants, among others [25].

3 Modeling of crystallization kinetics

During the thermoforming process of CoFRTP's containing a semi-crystalline matrix, the forming operation occurs while the matrix is in a molten state. In the context of modeling, it is therefore assumed that any stresses that arise during the forming operation quickly dissipate after the completion of the forming process, due to the very short relaxation times of the molten material. Further, it is assumed that as the melt continues to cool, the crystallization process begins and proceeds in a stress-free state. To define the physical state of the material (solid or fluid), a single scalar internal variable, X_c (absolute degree of crystallinity of the matrix), is used, with X_c being 0 in the molten state and some finite value, between 0 and 1, in the solid state. Section 5 provides additional details regarding the range of temperatures required for thermoforming CoFRTP composites with a PA6 matrix.

From a modeling perspective, the process of melt cooling and crystallization, which starts soon after forming when $\dot{X}_c \geq 0$, σ (2nd PK stress) $= 0$ is separated from the forming and post-crystallization processes, where $\dot{X}_c = 0$ and σ can be arbitrary.

The objective of this particular contribution is to evaluate the degrees of crystallinity in the laminate, which, as per the mentioned assumption, are unaffected by the stress state. For this purpose, the Helmholtz free energy function chosen by Felder [12] is simplified to the following form and adapted for the composite material

$$\psi = (1 - v_f)\, \psi_{X_c}(X_c, T) + \psi_c(T). \tag{1}$$

Here, v_f is the fiber volume fraction of the composite. The specific free energy of crystallization, or chemical potential, is denoted by $\psi_{X_c}(X_c, T)$ and the caloric contribution is denoted by $\psi_c(T)$. The fibers are not subjected to crystallization and it is assumed that they do not affect the crystallization of the matrix through nucleation or any other means.

To obtain the heat generation terms related to latent heat caused by crystallization, the local form of energy balance in the current configuration is analyzed

$$\rho_c \left(\dot{\psi} + \dot{s}T + s\dot{T}\right) + \mathrm{div}(\boldsymbol{q}) = 0. \tag{2}$$

Here, ρ_c is the density of the composite material, s is specific entropy and $\boldsymbol{q}$ is the heat flux vector in the current configuration. The expression is simplified by introducing the total time derivative of the Helmholtz free energy (1) and the time derivative of the specific entropy derived from Coleman and Noll's standard argument as $\dot{s} = -\partial\dot{\psi}/\partial T$ (see (10)). The resulting heat transfer equation is expressed in the following form

$$\rho_c \, c_T \, \dot{T} = \rho_c \left(-\frac{\partial \psi}{\partial X_c} + T\frac{\partial^2 \psi}{\partial X_c, \partial T}\right)\dot{X}_c - \mathrm{div}(\boldsymbol{q}). \tag{3}$$

Here, the isobaric specific heat capacity $c_T = -T(\partial^2\psi/\partial T^2)$ is defined for the composite material. In this study, the heat capacity is assumed to be solely dependent on the temperature $c_T \approx c_T(T)$. Below is a restructured form of (3), which incorporates a heat source, r_{X_c}, due to crystallization

$$\rho_c c_T \dot{T} = -\mathrm{div}(\boldsymbol{q}) + r_{X_c} \tag{4}$$

with

$$r_{X_c} = \rho_c \left(-\frac{\partial \psi}{\partial X_c} + T\frac{\partial^2 \psi}{\partial X_c, \partial T}\right)\dot{X}_c. \tag{5}$$

The Helmholtz free energy associated with crystallization (from [12]) is also adapted for composites as follows

$$\psi_{X_c}(X_c, T) = \frac{\rho_m}{\rho_c}\,\Delta h_f^{100}\frac{T - T_{\mathrm{on}}}{T_{\mathrm{on}}}\,X_c. \tag{6}$$

Here, ρ_m represents the density of the matrix material in the current configuration, Δh_f^{100} is the theoretical melting enthalpy of 100% crystalline matrix material and T_{on} is the start temperature of crystallization. The value of Δh_f^{100} is taken as 190 J/g [28]. After substituting the free energy (6) in (5) and simplifying, the following expression is derived for the heat source

$$r_{X_c} = \rho_m \, \Delta h_f^{100} \, \dot{X}_c \, (1 - v_f). \tag{7}$$

The constitutive relations are derived in a thermodynamically consistent manner based on the Clausius-Duhem form of entropy inequality. The Clausius-Duhem inequality under vanishing stress for the composite material in the current configuration is given by

$$-\rho_c \left(\dot{\psi} + s\dot{T}\right) - \frac{1}{T}\boldsymbol{q} \cdot \mathrm{grad}\,(T) \geq 0. \tag{8}$$

By taking the time derivative of the Helmholtz free energy (1) and substituting it into (8), the resulting expression is as follows

$$-\frac{1}{T}\boldsymbol{q} \cdot \mathrm{grad}\,(T) - \rho_c \left(\frac{\partial \psi}{\partial T} + s\right)\dot{T} - \rho_c \frac{\partial \psi}{\partial X_c}\dot{X}_c \geq 0. \tag{9}$$

This inequality has to be fulfilled for arbitrary values of the temperature rate, $\dot{T}$; hence the following expression is derived for the specific entropy s,

$$s = -\frac{\partial \psi}{\partial T}. \tag{10}$$

With this, the entropy inequality reduces to the following dissipation mechanism

$$-\frac{1}{T}\boldsymbol{q} \cdot \mathrm{grad}\,(T) - \rho_c \frac{\partial \psi}{\partial X_c}\dot{X}_c \geq 0. \tag{11}$$

The first term of (11) is fulfilled by Fourier's law, $\boldsymbol{q} = -\boldsymbol{\lambda_c}\,\mathrm{grad}\,(T)$, where $\boldsymbol{\lambda_c} = \lambda_{c_i}(e_i \otimes e_i)$ represents the orthotropic thermal conductivity of the composite material. In the second term of (11), as $\dot{X}_c \geq 0$, the term $\rho_c(\partial\psi/\partial X_c)$ remains negative as long as $T < T_{\mathrm{on}}$, considering (6). Thus, in this manner, the complete entropy inequality is fulfilled.

Next, an equation must be chosen to define the time evolution of the absolute degree of crystallinity, X_c, while ensuring that $\dot{X}_c \geq 0$. Due to the significant impact of crystallization on the structure and properties of polymeric materials, numerous approaches for modeling X_c are available in the literature. Notably, the Avrami equation [29] is a well-established method for modeling crystallization under isothermal conditions. However, during thermoforming, the material undergoes continuous cooling, resulting in non-isothermal crystallization in the matrix. Consequently, the Avrami model is not sufficient and there is a need for a more advanced approach. To this end, several authors, including Osawa [30], Nakamura [31], Ziabicki [32], Billon [33], Patel [34], Guo and Isayec [35], have extended the Avrami model to capture non-isothermal crystallization. Recent studies by Kugele [16] and Dörr [6] suggest that a combined formulation of the approaches from Nakamura [30] and Ziabicki [36], as used by Hoffman [37] and Sierra [38], is the best-suited model for capturing experimentally observed crystallization behavior over a wide range of cooling rates in semi-crystalline polymers. Thus, this approach is adopted in the present study. The expression for the relative crystallinity in this approach, as given by Nakamura [31], is

$$X_{cR} = 1 - \exp\left[-\left(\int_{t_{\text{on}}}^{t} K_c \, dt\right)^n\right]. \tag{12}$$

Here, t_{on} is the time at the crystallization onset. The crystallization constant, K_c, as given by Ziabicki [32], is

$$K_c = K_{\max} \exp\left(\frac{-4 \ln(2) \, (T - T_{\max})^2}{D^2}\right). \tag{13}$$

Here, $K_{\max}$, $T_{\max}$ and D are the cooling rate-specific parameters of the model. The evolution equation for the absolute crystallinity is derived by taking the time derivative of (12) and multiplying the resulting equation by the ratio $\Delta h_m / \Delta h_f^{100}$ as,

$$\dot{X}_c = n \; K_c \; (1 - X_{cR}) \left(\int_{t_{\text{on}}}^{t} K_c \, dt\right)^{(n-1)} \frac{\Delta h_m}{\Delta h_f^{100}}. \tag{14}$$

Here, Δh_m represents the enthalpy of fusion at the corresponding cooling rate.

4 Parameter identification

The S-DSC and F-DSC measurements outlined in Section 3 are adopted for parameter identification. In the modified Nakamura–Ziabicki model, the crystallization constant, given by (13), is represented by a Gaussian bell-shaped function with $K_{\max}$, $T_{\max}$ and D as unknown parameters. $T_{\max}$ is the temperature at the location of the peak maximum (typically center of the bell-curve). $K_{\max}$ represents the height of the crystallization curve and D is the width at the location $0.5\,K_{\max}$. The crystallization constant as a function of temperature is illustrated in Fig. 5.

The parameters are identified separately for each cooling rate by fitting the model to the relative crystallinity, X_{cR}, obtained from the DSC results. X_{cR} varies between 0 (when the material is molten) to 1 (when the material

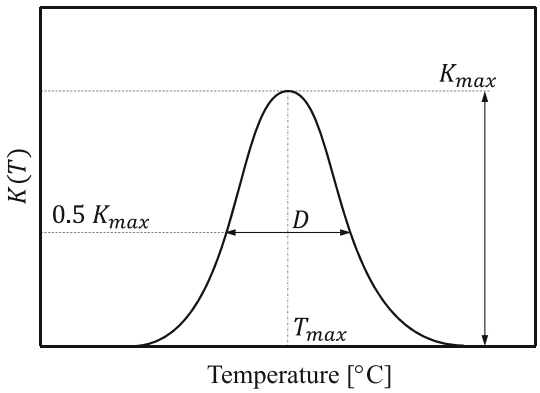

Fig. 5 Schematic representation of the peak function of the crystallization constant with the required model parameters according to [37,39]

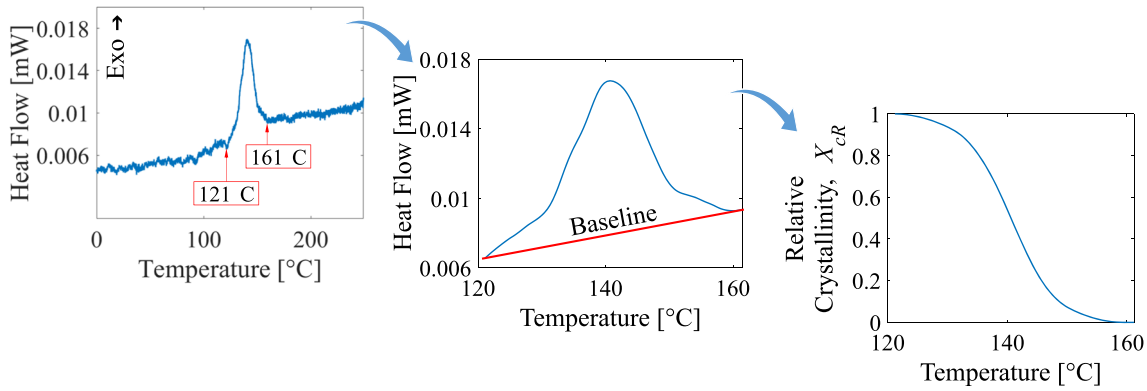

Fig. 6 An approach to extract the relative crystallinity from the DSC curve, shown here for a F-DSC cooling signal of 50 °C/s: First, choosing the crystallization zone, then integrating the peak

is fully crystallized). The relative crystallinity, X_{c_R}, is derived from the heat flow signal as follows. First, since only the latent heat signal is of interest, only the bell-shaped part of the heat flow signal is considered. The start and end points of the latent heat curve are chosen where a pronounced alteration in the signal's slope is observed, as seen in Fig. 6. Then the latent heat flux is integrated over temperature at all measurement data points starting at the highest temperature; integration was done numerically using the trapezoidal rule. The integration results at each time step were divided by the total area under the bell-shaped curve to get the quantity X_{c_R} according to (15).

$$X_{c_R}(t) = \frac{\int_{t_{\text{on}}}^{t} \dot{q}\, dt}{\Delta q_c} \tag{15}$$

Here, $\dot{q}$ is the latent heat flow signal and Δq_c is the total area under the bell-shaped curve. The way in which the heat flow signal data is transformed to X_{c_R} is shown in Fig. 6.

The parameter $T_{\max}$ is determined manually as the peak temperature of the bell-shaped curve. The parameters, $K_{\max}$ and half-width D, are then identified by solving the least square objective function using the Levenberg-Marquardt algorithm in MATLAB. Appendix 6 contains the plots of the parameters acquired through the fitting. Avrami index n, which contains information about nucleation and growth geometry [6], has been normally calculated in the literature based on isothermal crystallization experiments. In the scope of this project, no isothermal experiments were performed and hence n was chosen manually as 3 to achieve an optimal fit visually. The F-DSC results were fitted for cooling rates of 5 °C s^{-1} and greater, as the signal-to-noise ratio was inadequate for slower cooling rates. On the other hand, the S-DSC results were fitted over a range of 0.033 to 0.25 °C s^{-1} until the curves appeared fairly symmetrical, ensuring the fidelity of the results. Figure 7 depicts the fitting results for X_{c_R}, with n set at 3.

The experiment and the model show strong agreement, demonstrating that the modified Nakamura–Ziabicki model is well-suited for a broad range of cooling rates. To estimate the parameter values for the unknown cooling rates in between, linear regression is used.

The enthalpy of crystallization (Δh_m) for the S-DSC results is calculated by integrating the crystallization bell-curves of the cooling heat flow signal. However, for F-DSC, it is to be noted that, since the mass of the F-DSC specimens is unknown, it is not possible to determine the absolute enthalpy of crystallization or melting using F-DSC data alone. Hence, to calculate Δh_m, the areas under the F-DSC heating bell curves were first normalized using a reference slow cooling rate of 0.25 °C s^{-1} as a basis with a value of 1. Δh_m for the 0.25 °C s^{-1} cooling rate is already evaluated from the S-DSC, which was 57.9 J g^{-1}. The normalized values were then multiplied by 57.9 J g^{-1} to compute the Δh_m for the F-DSC results. Figure 14d shows the Δh_m values calculated based on the F-DSC results.

5 FE simulations

The objective of these simulations is two-fold: firstly, to examine the initiation and progression of the crystallinity distribution in the thickness direction of a laminate and secondly, to investigate the influence of

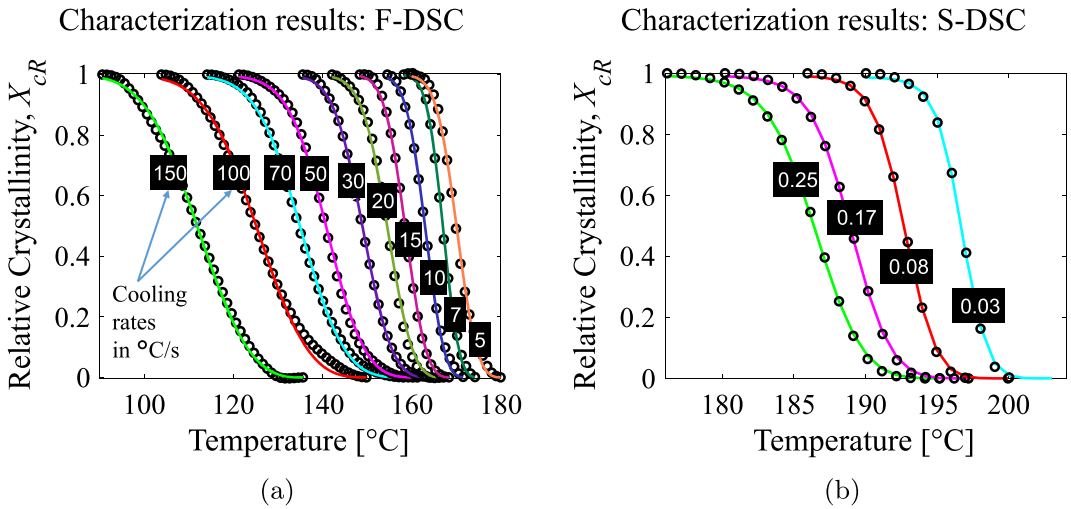

Fig. 7 Comparison of relative crystallinities (X_{c_R}) determined from DSC results with the fitted model, **a** F-DSC characterization results, **b** S-DSC characterization results

exothermic latent heat flows that are dependent on the cooling rates on the temperature field during the consolidation (cooling) phase of the thermoforming process. The thermoforming or thermostamping process for CoFRTP works as follows. First, a pre-consolidated composite laminate is heated well above the melting temperature of the semi-crystalline polymer. Then the laminate, in its gell-form, is quickly transferred to the dies and formed at a pre-defined speed. The dies are initially at a significantly lower temperature than the laminate. During transfer and forming, the temperature of the laminate continuously decreases due to heat dissipation through convection to the surrounding air and conduction through contact surfaces between the dies and the laminate. The closing of dies is usually displacement-controlled. The formed part is then cooled/consolidated while the pressure is applied. During this consolidation step, the heat transfer from the laminate takes place predominantly through conduction as the laminate is entirely in contact with the dies. After being cooled for 20 to 60 s, the component is finally extracted.

The material examined in this study is a unidirectional, continuous fiber-reinforced thermoplastic composite consisting of glass fibers and a PA6 matrix. The composite has a fiber volume content of 40% and a density of 1.80 g cm^{-3} at room temperature.

The selected material in the thermoforming process is typically heated in the IR oven to between 280 and 290 °C (T_m of PA6 is nearly 220 °C) [8,39,40]. Heating the material above 300 °C is avoided, as material degradation occurs immediately [8]. The transfer to the moulding station and initial punch speed should be fast enough such that the laminate temperature is still in the forming temperature range of 240–280 °C as recommended by LANXESS. This temperature is well above the solidification/crystallization temperature of PA6, which is typically below 200 °C, as observed in the DSC results (Figs. 1 and 3). After the forming step is finished, the laminate cools under a constant transverse pressure of approximately 5 bar until it solidifies and reaches the die temperature. The recommended die temperature is typically less than 100 °C.

As the main interest is to analyze the crystallinity evolution from melt cooling, the simulation is initiated from the beginning of the consolidation step, when the forming operation is just finished and the composite melt is stationary and is completely in contact with the dies. The cooling rates during crystallization depend upon several factors, such as initial laminate temperature, die temperature, die travel speed, laminate thickness etc. The initial tool-laminate contact causes high local cooling rates and hence a strong local inhomogeneity of the crystallinity distribution in the laminate. It is, therefore, conceivable that certain regions on the laminate surface may undergo crystallization during the forming process, as per the findings of [8]. However, the likelihood of this event is excluded in the current simulation as the LANXESS guidelines recommend a significant temperature difference of at least 40 °C between the forming and crystallization stages. Thus, the simulation assumes that the entire material is initially in a molten state and has a uniform temperature at the start of the consolidation phase. To examine the impact of a broad spectrum of possible cooling rates, two initial laminate temperature cases are analyzed: 200 °C and 250 °C. Also, three different laminate thicknesses are studied: 1 mm, 2 mm and 3 mm. The simulation setup is explained in the following.

The simulation was performed with the commercial software COMSOL Multiphysics® in 2D. In this simulation, solely the temperature field was solved while neglecting the mechanical effects. The geometry

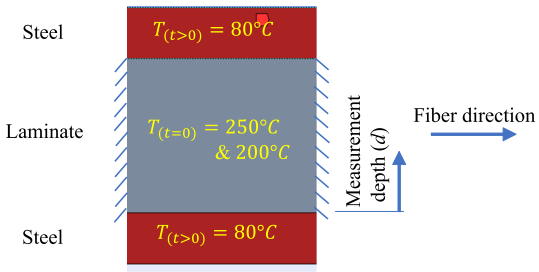

Fig. 8 The boundary value problem for the simulation of the consolidation phase during thermoforming

and boundary conditions are illustrated in Fig. 8. A 1-D simulation would also have been sufficient as the heat transfer in the transverse direction is the main focus of the simulation; however, a 2D simulation was done to get better visuals of the result. A composite is modeled as a homogeneous layer located between two steel plates of thickness 10 mm each which represent the dies. In Fig. 8, the dies are only partly depicted. The dies have an initial homogeneous temperature of 80 °C. It is noteworthy that the thermal conductivity of a unidirectional composite is supposed to be anisotropic and, therefore, the conductivity perpendicular to the fiber direction (in the thickness direction) was used. Perfect thermal contact is assumed between the laminate and the dies, which implies that the heat transfer coefficient between the laminate and the dies is theoretically infinite. The initial temperature of the laminate is considered homogeneous, as stated before. Only the heat transfer due to conduction is considered, while the heat transfer due to air convection from the dies and radiation is neglected.

The thermal conductivity of the composite in the direction perpendicular to the fiber direction $\lambda_c^{\perp}$ is determined using the rule of mixture as given by (16). The rule assumes that there is perfect contact between the fibers and the matrix. The rule was proposed by Hasselman [41] and has recently been employed by Dörr [6] and Guzman [10] in thermoforming simulations.

$$\lambda_c^{\perp} = \lambda_m \frac{\left(\frac{\lambda_f^{\perp}}{\lambda_m} - 1\right) v_f + \left(1 + \frac{\lambda_f^{\perp}}{\lambda_m}\right)}{\left(1 - \frac{\lambda_f^{\perp}}{\lambda_m}\right) v_f + \left(1 + \frac{\lambda_f^{\perp}}{\lambda_m}\right)} \tag{16}$$

Here, $\lambda_f^{\perp}$ represents the thermal conductivity of the fibers in the radial direction, λ_m represents the isotropic thermal conductivity of the matrix and v_f represents the volume fraction of fibers. In a previous study by Kugele [39], the thermal conductivity of a similar unidirectionally reinforced composite was measured in the direction transverse to the fibers. The difference between the thermal conductivity at two temperatures, 23 °C and 275 °C, was found to be only 0.15 W $m^{-1}K^{-1}$, which is considered too small to impact the resulting temperature field significantly. Therefore, for the purposes of this simulation, a constant thermal conductivity is assumed across all temperatures. λ_m for PA6 was measured at 130 °C using an in-house Hot disc device TPS 2500 S and was found to be λ_m=0.315 W $m^{-1}K^{-1}$. The E-glass fibers are considered to be isotropic ($\lambda_f^{\perp} = \lambda_f^{\parallel}$) with a thermal conductivity of 1.03 W $m^{-1}K^{-1}$ [42]. Using the rule of mixture (16), the resultant $\lambda_c^{\perp}$ is calculated to be 0.4858 W $m^{-1}K^{-1}$.

The density of the composite ρ_c according to the manufacturer is 1.80 g cm^{-3} at 23°C and is used for the simulation. For simplification, it is assumed that, in the overall cooling process, there is no change in density with respect to temperature or degree of crystallinity. During a transition from the melt state at 250 °C to solid state at 23 °C, the density of PA6 ρ_m increases by approximately 20% (from 0.94 g cm^{-3} to 1.13 g cm^{-3}). At a temperature of 23°C, the density of PA6 with $X_c = 29\%$ is 1.13 g cm^{-3}, whereas PA6 with $X_c = 14\%$ has a 6% lower density of 1.06 g cm^{-3}. While the effects of density variation are crucial for predicting the reduction in laminate thickness, they have not been considered in this study. This aspect will be explored in future research.

The isobaric heat capacity of a composite material c_T was measured under the supervision of Dr. André Wutzler at PSM Merseburg. During the measurement of the composite material, a near-linear correlation was observed between the heat capacity and the temperature. Hence, the heat capacity is approximated by the following relation

$$c_T \left[\frac{\mathrm{J}}{\mathrm{g\,K}}\right] = 0.0022 \left[\frac{\mathrm{J}}{\mathrm{g\,K^2}}\right] T\,[\mathrm{K}] + 0.7377 \left[\frac{\mathrm{J}}{\mathrm{g\,K}}\right]. \tag{17}$$

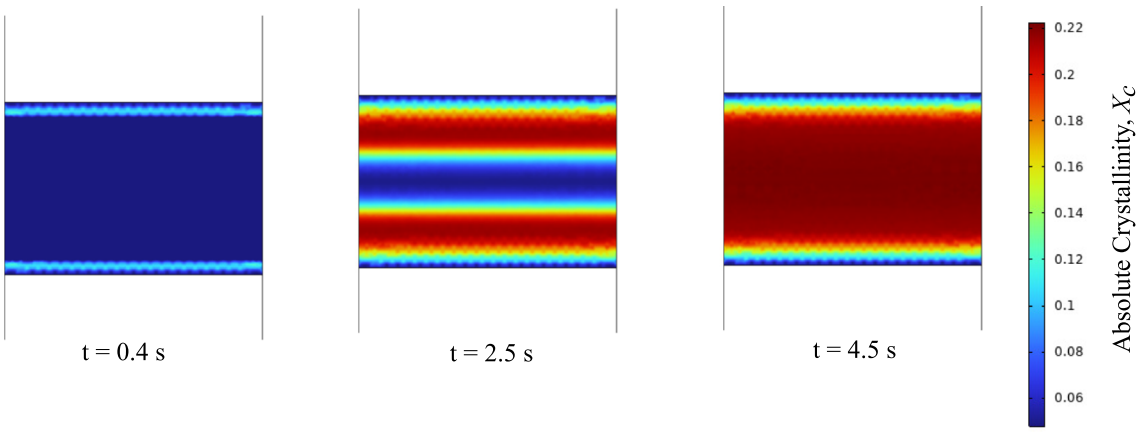

Fig. 9 Simulation result: time evolution of absolute crystallinity, X_c, of the matrix for the configuration $T_{\text{laminate}(t=0)} = 250\,^{\circ}\text{C}$ and laminate thickness = 2 mm

The steel dies have a thermal conductivity of 34.5 W $\text{m}^{-1}\text{K}^{-1}$, a specific heat capacity of 460 J $\text{kg}^{-1}\text{K}^{-1}$ and a density of 7830 kg m^{-3} [39].

A thermal simulation is performed for the setup explained above. In this simulation, the laminate thickness is 2 mm. The initial laminate temperature is 250 °C and the die temperature is 80 °C. The laminate is allowed to cool for 60 s. The absolute crystallinity of the material was plotted at various time intervals in Fig. 9.

As seen in Fig. 9, the absolute crystallinity of the matrix, X_c, reaches a maximum value of around 0.23 or 23% at 4.5 s and remains constant thereafter. It should be noted that crystallinity values are calculated based on a 100% crystallization enthalpy (Δh_f^{100}) of 190 J g^{-1}. Due to the high temperature gradient between the die and the laminate, the surface layer in direct contact with the die undergoes rapid cooling. As a result, a thin zone near the surface is observed, where there is a rapid transition in X_c (cf. Fig. 9).

Figure 10a displays the cooling rates at various depths when the local temperatures drop below the cooling rate-dependent crystallization onset temperatures (T_{on}) and crystallization is triggered. Figure 14e shows the cooling rate-dependent T_{on} for various cooling rates measured in the DSC. In the simulation, the heat source for crystallization (r_{X_c}) is activated at the nodal level to release the cooling rate-specific and time-dependent latent heat, as specified by (5). In Fig. 10b, the progression of X_c in the matrix at four different depths is demonstrated. The DSC results in Fig. 14d indicate that the latent heat of crystallization or melting decreases with an increase in cooling rates. Therefore, the surface layer, which experiences a higher cooling rate than the core region, has a lower X_c.

Despite a very high cooling rate of 210 °C s^{-1} on the surface, the matrix still does not become entirely amorphous. The transition to a completely amorphous material requires cooling rates higher than 1000 °C s^{-1}, as seen in the prior F-DSC experiments (Fig. 3).

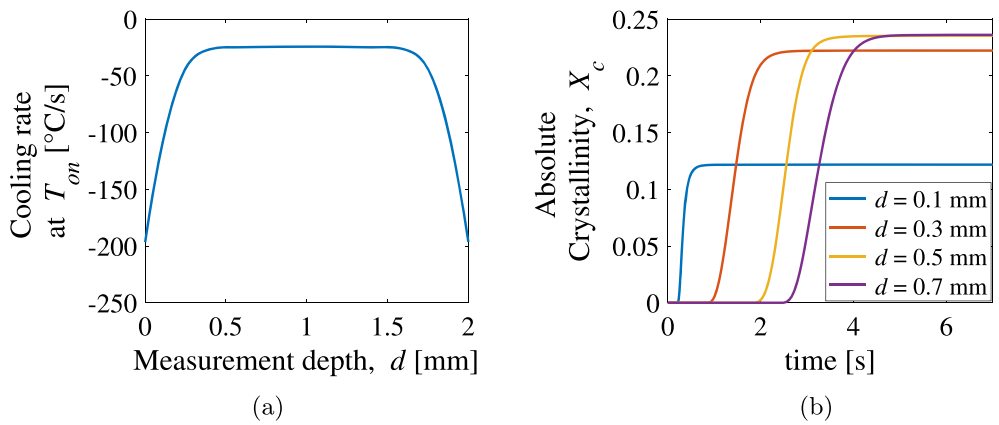

Fig. 10 Simulation results: **a** Plot of cooling rates at the onset of crystallization, T_{on}, over laminate depth, d. **b** Time evolution of absolute crystallinity of the matrix, X_c, at 4 different depths; for the configuration $T_{\text{laminate}(t=0)} = 250\,^{\circ}\text{C}$ and laminate thickness = 2 mm

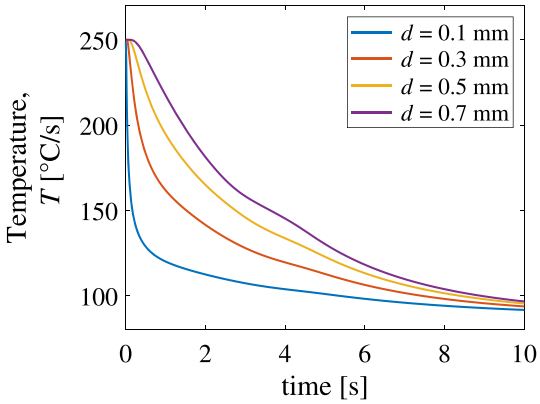

Fig. 11 Simulation results: Time evolution of temperature, T, at 4 different laminate depths, d, for the configuration $T_{\text{laminate}(t=0)} = 250\,°\text{C}$ and laminate thickness = 2 mm

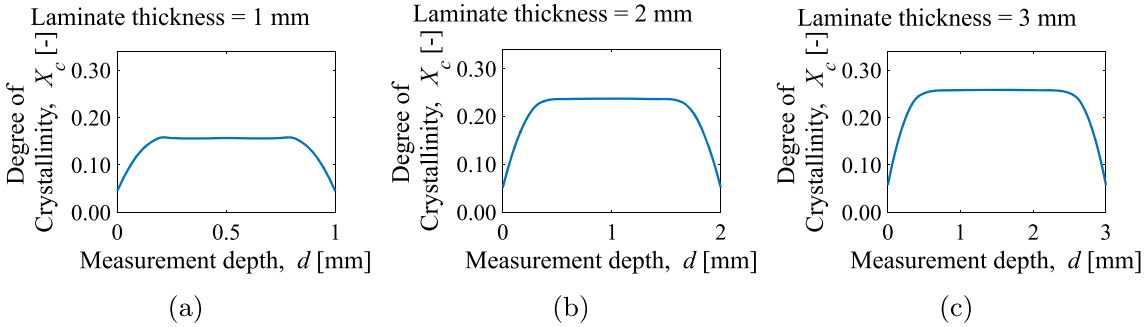

Fig. 12 Effect of laminate thickness on the final degree of crystallinity, X_c, of the matrix; $T_{\text{laminate}(t=0)} = 250\,°\text{C}$ and the result is measured at $t = 60\,\text{s}$

The resulting space- and time-dependent temperature field in the laminate is analyzed in Fig. 11. The core region's reduced cooling rates lead to the generation of larger latent heat exotherms, which counters the cooling effect to a larger extent. Therefore, the crystallization-induced alteration in the temperature profile is more pronounced in the core region.

5.1 Case study 1: Influence of laminate thickness on the resulting final degree of crystallinity of the matrix

In the first case study, simulations were conducted for two additional laminate thicknesses, namely 1 mm and 3 mm. The outcome of the absolute crystallinity, X_c, is displayed in Fig. 12 for all three laminates. In all three cases, the results show that X_c within the matrix progressed swiftly from a low value at the surface to a maximum value in the core region, where it remained roughly constant. X_c in the core region exhibits significant variation depending on the laminate thickness, ranging from 0.16 (16%) for a thickness of 1 mm to 0.26 (26%) for a thickness of 3 mm.

5.2 Case study 2: Influence of initial laminate temperature ($T_{\text{laminate}(t=0)}$) on the resulting final degree of crystallinity of the matrix

The temperature difference between the laminate and the dies is believed to be a critical process parameter in determining the cooling rate, which affects the local degree of crystallinity and hence the physical properties of the composite. Hence, in this case study an additional initial laminate temperature of 200 °C was investigated for a laminate with a thickness of 2 mm. Figure 13 displays the obtained results, which indicate that while the maximum of the X_c in the core remained constant, the core region's width decreased and the width of the transition region near the surface increased.

6 Summary and next steps

The study introduces an innovative simulation approach to assess the progression of the crystallization process and determine the temperature field during cooling in the thermoforming process for CoFRTP. The simulation

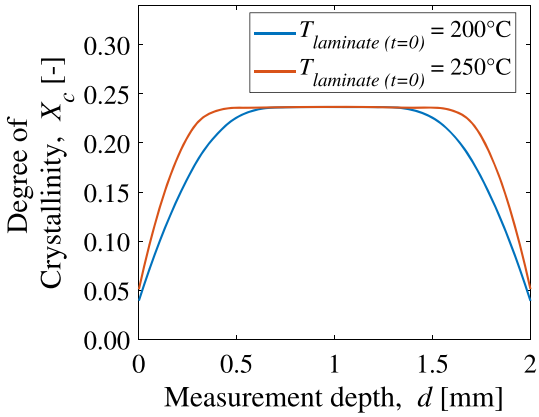

Fig. 13 Effect of initial laminate temperature, $T_{\text{laminate}(t=0)}$, on the final degree of crystallinity of the matrix, X_c; the laminate thickness is 2 mm

accounts for the complex interplay between the composite material's thermal and caloric properties, including exothermic latent heat flows that depend on the local cooling rates.

In this study, the crystallization behavior of the matrix material during cooling was experimentally investigated using differential scanning calorimetry (DSC). The cooling kinetics for moderate to high-temperature rates ranging from 0.25 to 3000 °C s^{-1} were studied using flash DSC, while low to moderate cooling rates from 0.033 to 1 °C s^{-1} were investigated using S-DSC. To model the non-isothermal crystallization kinetics, the modified Nakamura–Ziabicki model, an extended form of the Avrami model that has been successfully used by many authors, was employed. Overall, the modified Nakamura–Ziabicki model demonstrated good accuracy in predicting the non-isothermal crystallization behavior over the process-relevant range of cooling rates. In order to parametrize the modified Nakamura–Ziabicki model, a combination of S-DSC and F-DSC data was used. The resulting parameters, including $T_{\max}$, $K_{\max}$, D, Δh_m, T_{on}, showed a continuous and consistent trend between individual DSC measurements as well as between the two DSC measurements. This finding supports the suitability of the combined use of S-DSC and F-DSC results in characterizing the crystallization kinetics over a wide range of cooling rates spanning 4 decades.

The developed simulation methodology was used to explore the influence of laminate thickness and initial temperature on the degree of crystallinity of thermoformed laminates. The obtained results showed a considerable difference of approximately 10% in the final degree of crystallinity of the matrix between the thinnest and thickest laminates investigated (1 mm and 3 mm). With a decrease in the initial temperature from 250 to 200 °C, although the core region's degree of crystallinity remained stable, the width of the transition layer near the surface increased.

The simplified simulation model used in this study assumes that the laminate is in perfect contact with the dies and disregards the effects of mechanical pressure. But it's important to note that contact nonuniformities, variations in the contact pressure and contact conductance over the surface of the laminate may lead to differences in the results obtained. In addition, the skin-core effect [43], which involves changes in the thickness of the outer skin layer due to variations in initial melt temperature and subsequently impacts the crystallinity of the core region, has not been investigated. To evaluate the impact of these effects, a composite cooling experiment will be conducted to validate the model developed in this project.

The solid-state mechanical properties of a laminate are significantly affected by the degree of crystallinity, which can vary by tens of percent, as observed in the current study. Therefore, the development of a constitutive model for composites that incorporates the process-induced degree of crystallinity as a variable is essential for accurately predicting residual stresses and warping in the resulting component. The ongoing research project aims to develop such a model, which can also be used to predict the material response of laminates under field loads during their service life.

Acknowledgements We wish to acknowledge the support provided by the DFG towards this research. Furthermore, we would like to express our gratitude to Professor René Androsch from the University of Halle, Germany and Dr. André Wutzler from PSM Merseburg, Germany, for conducting the F-DSC experiments and specific heat capacity measurement, respectively.

Funding Open Access funding enabled and organized by Projekt DEAL.

Appendix A Model parameters

See Fig. 14.

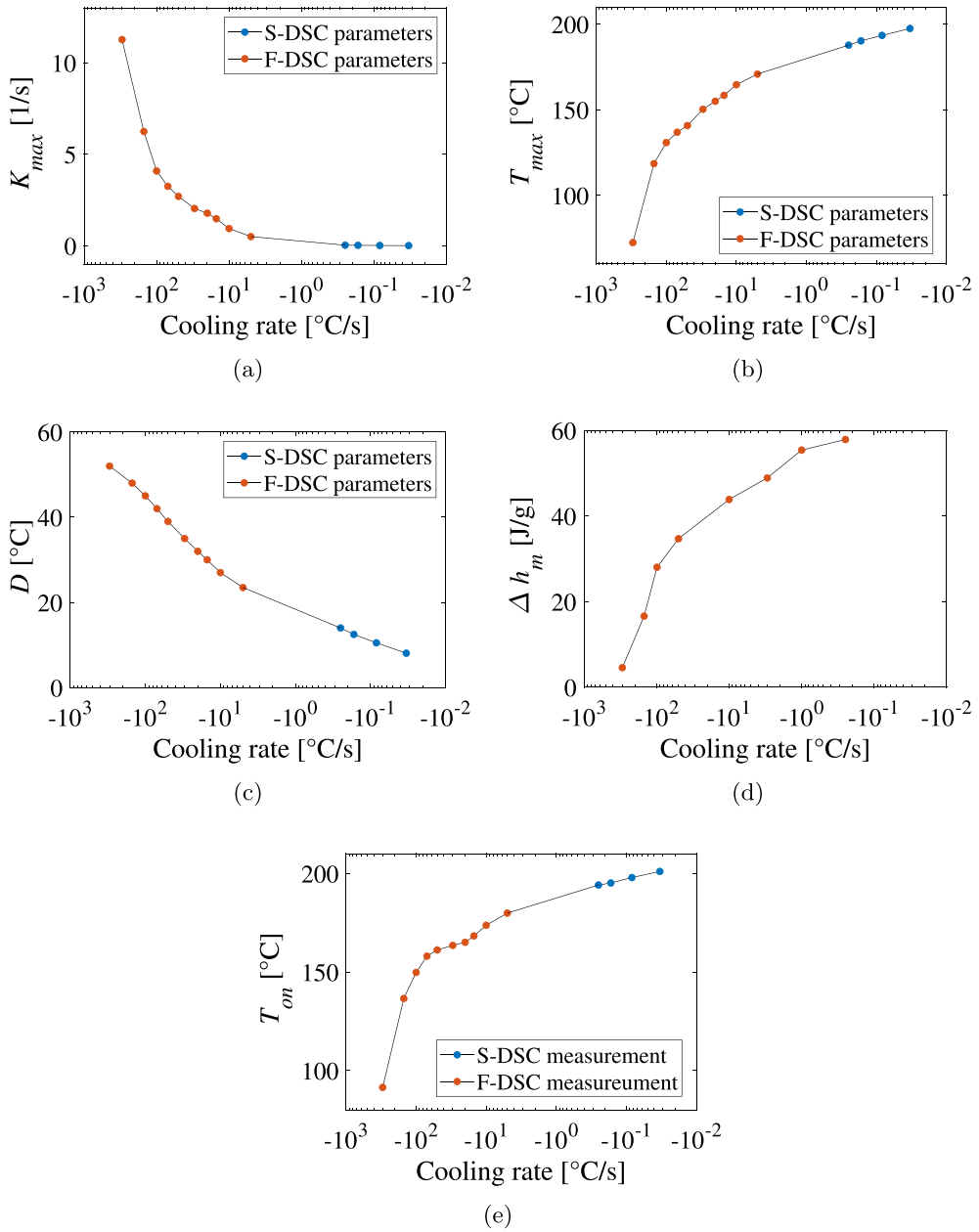

Fig. 14 Parameters of the Nakamura–Ziabicki model: **a** $K_{\max}$, **b** $T_{\max}$, **c** D and DSC results: **d** Enthalpy of fusion (Δh_m), **e** Crystallization onset temperature (T_{on})

References

1. Zhou, W.D., Chen, J.S.: 3d printing of carbon fiber reinforced plastics and their applications. Mater. Sci. Forum **913**, 558–563 (2018). https://doi.org/10.4028/www.scientific.net/MSF.913.558
2. Henning, F., Kärger, L., Dörr, D., Schirmaier, F.J., Seuffert, J., Bernath, A.: Fast processing and continuous simulation of automotive structural composite components. Compos. Sci. Technol. **171**, 261–279 (2019). https://doi.org/10.1016/j.compscitech.2018.12.007
3. Chen, H., Li, S., Wang, J., Ding, A.: A focused review on the thermo-stamping process and simulation progresses of continuous fibre reinforced thermoplastic composites. Compos. B Eng. **224**, 109196 (2021). https://doi.org/10.1016/j.compositesb.2021.109196
4. Friedrich, K., Hou, M., Krebs, J.: Chapter 4 thermoforming of continuous fibre/thermoplastic composite sheets. In: Composite Sheet Forming. Composite Materials Series, 11, pp. 91–162. Elsevier, Amsterdam (1997). https://doi.org/10.1016/S0927-0108(97)80006-9
5. Guzman-Maldonado, E., Hamila, N., Boisse, P., Bikard, J.: Thermomechanical analysis, modelling and simulation of the forming of pre-impregnated thermoplastics composites. Compos. A Appl. Sci. Manuf. **78**, 211–222 (2015). https://doi.org/10.1016/j.compositesa.2015.08.017
6. Dörr, D.: Simulation of the thermoforming process of UD fiber-reinforced thermoplastic tape laminates. Karlsruhe. https://doi.org/10.5445/IR/1000099485
7. Guzman-Maldonado, E., Hamila, N., Wang, P., Boisse, P.: Thermoforming of fiber–plastic composites: mechanical tests and simulations. In: Encyclopedia of Polymer Science and Technology, pp. 1–19. Wiley, Hoboken (2002). https://doi.org/10.1002/0471440264.pst371.pub2
8. Joppich, T.D.: Beitrag zum Umformverhalten von PA6/CF Gelegelaminaten im nicht-isothermen Stempelumformprozess. Karlsruhe. https://doi.org/10.5445/IR/1000097015
9. Machado, M., Murenu, L., Fischlschweiger, M., Major, Z.: Analysis of the thermomechanical shear behaviour of woven-reinforced thermoplastic-matrix composites during forming. Compos. A Appl. Sci. Manuf. **86**, 39–48 (2016). https://doi.org/10.1016/j.compositesa.2016.03.032
10. Guzman-Maldonado, E., Hamila, N., Naouar, N., Moulin, G., Boisse, P.: Simulation of thermoplastic prepreg thermoforming based on a visco-hyperelastic model and a thermal homogenization. Mater. Des. **93**, 431–442 (2016). https://doi.org/10.1016/j.matdes.2015.12.166
11. Parodi, E., Peters, G.W.M., Govaert, L.E.: Structure–properties relations for polyamide 6, part 1: influence of the thermal history during compression moulding on deformation and failure kinetics. Polymers (2018). https://doi.org/10.3390/polym10070710
12. Felder, S., Holthusen, H., Hesseler, S., Pohlkemper, F., Gries, T., Simon, J.-W., Reese, S.: Incorporating crystallinity distributions into a thermo-mechanically coupled constitutive model for semi-crystalline polymers. Int. J. Plast. **135**, 102751 (2020). https://doi.org/10.1016/j.ijplas.2020.102751
13. Schawe, J.E.K.: Cooling rate dependence of the crystallinity at nonisothermal crystallization of polymers: a phenomenological model. J. Appl. Polym. Sci. (2016). https://doi.org/10.1002/app.42977
14. Kulkarni, S., Loos, K., Lion, A., Johlitz, M.: Thermoforming: identification of process-relevant ranges for strain, strain rate, cooling rate, and degree of crystallinity through preliminary simulations. In: Altenbach, H., Johlitz, M., Merkel, M., Öchsner, A. (eds.) Lectures Notes on Advanced Structured Materials. Advanced Structured Materials, vol. 153, pp. 303–314. Springer, Cham (2022). https://doi.org/10.1007/978-3-031-11589-9
15. Reuvers, M., Boes, B., Felder, S., Brepols, T., Reese, S.: A thermo-coupled constitutive model for semi-crystalline polymers at finite strains: application to varying degrees of crystallinity and temperatures. In: 8th European Congress on Computational Methods in Applied Sciences and Engineering. CIMNE, Barcelona (5th-9th June 2022). https://doi.org/10.23967/eccomas.2022.030
16. Kugele, D., Dörr, D., Wittemann, F., Hangs, B., Rausch, J., Kärger, L., Henning, F.: Modeling of the non-isothermal crystallization kinetics of polyamide 6 composites during thermoforming. In: ESAFORM 2017, p. 030005. AIP Conference Proceedings 1896, Dublin, Ireland (26–28 April 2017). https://doi.org/10.1063/1.5007992
17. Descher, S., Wünsch, O.: Simulation framework for crystallization in melt flows of semi-crystalline polymers based on phenomenological models. Arch. Appl. Mech. **92**(6), 1859–1878 (2022). https://doi.org/10.1007/s00419-022-02153-x
18. Schawe, J.E.K.: Practical aspects of the flash dsc 1: sample preparataion for measurements of polymers. Mettler Toledo Therm. Anal. UserCom **36**, 17–24 (2012)
19. Schawe, J.E.K.: Flash dsc 1: a novel fast differential scanning calorimeter. (2011). https://doi.org/10.13140/RG.2.1.2062.6641
20. Millot, C., Fillot, L.-A., Lame, O., Sotta, P., Seguela, R.: Assessment of polyamide-6 crystallinity by dsc. J. Therm. Anal. Calorim. **122**(1), 307–314 (2015). https://doi.org/10.1007/s10973-015-4670-5
21. Mileva, D., Kolesov, I., Androsch, R.: Morphology of cold-crystallized polyamide 6. Colloid Polym. Sci. **290**(10), 971–978 (2012). https://doi.org/10.1007/s00396-012-2657-3
22. Khanna, Y.P., Kuhn, W.P.: Measurement of crystalline index in nylons by dsc: complexities and recommendations. J. Polym. Sci. Part B Polym. Phys. **35**(14), 2219–2231 (1997). https://doi.org/10.1002/(SICI)1099-0488(199710)35:142219::AID-POLB3
23. Schawe, J.E.K.: Influence of processing conditions on polymer crystallization measured by fast scanning dsc. J. Therm. Anal. Calorim. **116**(3), 1165–1173 (2014). https://doi.org/10.1007/s10973-013-3563-8
24. Furushima, Y., Nakada, M., Ishikiriyama, K., Toda, A., Androsch, R., Zhuravlev, E., Schick, C.: Two crystal populations with different melting/reorganization kinetics of isothermally crystallized polyamide 6. J. Polym. Sci. Part B Polym. Phys. **54**(20), 2126–2138 (2016). https://doi.org/10.1002/polb.24123
25. Mathot, V., Pyda, M., Pijpers, T., Vanden Poel, G., van de Kerkhof, E., van Herwaarden, S., van Herwaarden, F., Leenaers, A.: The flash dsc 1, a power compensation twin-type, chip-based fast scanning calorimeter (fsc): first findings on polymers. Thermochim. Acta **522**(1–2), 36–45 (2011). https://doi.org/10.1016/j.tca.2011.02.031

26. Kolesov, I., Mileva, D., Androsch, R., Schick, C.: Structure formation of polyamide 6 from the glassy state by fast scanning chip calorimetry. Polymer **52**(22), 5156–5165 (2011). https://doi.org/10.1016/j.polymer.2011.09.007
27. Parodi, E., Govaert, L.E., Peters, G.W.M.: Glass transition temperature versus structure of polyamide 6: a flash-dsc study. Thermochim. Acta **657**, 110–122 (2017). https://doi.org/10.1016/j.tca.2017.09.021
28. Hammami, I., Hammami, H., Soulestin, J., Arous, M., Kallel, A.: Thermal and dielectric behavior of polyamide-6/clay nanocomposites. Mater. Chem. Phys. **232**, 99–108 (2019). https://doi.org/10.1016/j.matchemphys.2019.04.048
29. Avrami, M.: Kinetics of phase change. I general theory. J. Chem. Phys. **7**(12), 1103–1112 (1939). https://doi.org/10.1063/1.1750380
30. Ozawa, T.: Kinetics of non-isothermal crystallization. Polymer **12**(3), 150–158 (1971). https://doi.org/10.1016/0032-3861(71)90041-3
31. Nakamura, K., Watanabe, T., Katayama, K., Amano, T.: Some aspects of nonisothermal crystallization of polymers. I. relationship between crystallization temperature, crystallinity, and cooling conditions. J. Appl. Polym. Sci. **16**(5), 1077–1091 (1972). https://doi.org/10.1002/app.1972.070160503
32. Ziabicki, A.: Fundamentals of Fibre Formation: The Science of Fibre Spinning and Drawing. Wiley, London (1976)
33. Billon, N., Barq, P., Haudin, J.M.: Modelling of the cooling of semi-crystalline polymers during their processing. Int. Polym. Proc. **6**(4), 348–355 (1991). https://doi.org/10.3139/217.910348
34. Patel, R.M., Spruiell, J.E.: Crystallization kinetics during polymer processing: analysis of available approaches for process modeling. Polym. Eng. Sci. **31**(10), 730–738 (1991). https://doi.org/10.1002/pen.760311008
35. Guo, X., Isayev, A.I., Guo, L.: Crystallinity and microstructure in injection moldings of isotactic polypropylenes. Part 1. A new approach to modeling and model parameters. Polym. Eng. Sci. **39**(10), 2096–2114 (1999). https://doi.org/10.1002/pen.11601
36. Hoffman, J.D., Davis, G.T., Lauritzen, J.I.: The rate of crystallization of linear polymers with chain folding. In: Hannay, N.B. (ed.) Treatise on Solid State Chemistry, pp. 497–614. Springer, Boston (1976). https://doi.org/10.1007/978-1-4684-2664-9
37. Hoffmann, S.: Berechnung Von Kristallisationsvorgängen in Kunststoffformteilen: = Calculation of Crystallisation in Thermoplastic Mouldings: Zugl.: Aachen, Techn. Hochsch., Diss., 2002, 1. aufl. edn. IKV-Berichte aus der Kunststoffverarbeitung, vol. Bd. 136. Mainz, Aachen (2003)
38. Sierra, J.D., Noriega, M.P., Gomez, J.F., Pastor, J.M.: Isothermal and nonisothermal crystallization kinetics for blends of polyamide 6 and polypropylene. J. Plast. Technol. **5**, 1–21 (2006)
39. Kugele, D.: Experimentelle und numerische Untersuchung des Abkühlverhaltens thermoplastischer Gelegelaminate in der Prozesskette. Karlsruhe. https://doi.org/10.5445/IR/1000122371
40. Schug, A.F.: Unidirectional Fibre Reinforced Thermoplastic Composites: A Forming Study. Universitätsbibliothek der TU München, München (2020)
41. Hasselman, D.P.H., Donaldson, K.Y., Thomas, J.R.: Effective thermal conductivity of uniaxial composite with cylindrically orthotropic carbon fibers and interfacial thermal barrier. J. Compos. Mater. **27**(6), 637–644 (1993). https://doi.org/10.1177/002199839302700605
42. Lin, W.-Q., Zhang, Y.-X., Wang, H.: Thermal conductivity of unidirectional composites consisting of randomly dispersed glass fibers and temperature-dependent polyethylene matrix. Sci. Eng. Compos. Mater. **26**(1), 412–422 (2019). https://doi.org/10.1515/secm-2019-0024
43. Murthy, N.S., Kagan, V.A., Bray, R.G.: Effect of melt temperature and skin-core morphology on the mechanical performance of nylon 6. Polym. Eng. Sci. **42**(5), 940–950 (2002). https://doi.org/10.1002/pen.11003